Supporting Information

3.2. Instrumentation employed for methods of charachterization

All melting points were recorded on the Melt-Temp II melting point apparatus. IR spectra were measured as KBr pellets on a Shimadzu DR-8001 spectrometer. ^{1}H, ^{13}C NMR spectra were recorded on a Bruker DRX 400 MHz using TMS as an internal reference and DMSO as a solvent. All compounds were checked for their purity on TLC plates. By using model T+80 of PG spectrophotometer in Ethanol as a solvent were detected UV-Vis spectra of the ligand and its complexes at 298 K were detected at the University of Sohag, Faculty of Science in the Department of Chemistry. The elemental [C, H & N] analyses were done at the Central Laboratory, University of Zagazig, by a [Perkin-Elmer 2408] analyzer. By using Model 60 H Shimadzu analyzer for thermo gravimetric analysis and determining the parameters of thermo-kinetic activation of synthesized complexes in air and at a heating rate of 10 $^{o}C\ min^{-1}$ in the Department of Chemistry, Faculty of Science, Thermal Analysis Unit, the University of Cairo, Egypt. For the estimation of the molar conductance of the complexes at 298K. By utilizing model 4320 of the conductivity meter [JENWAY] in DMF as a solvent. By using the Elico digital [model LI-127] pH meter comes with a [CL-51B] combined electrode for pH evaluation, and before evaluations might be calibrated vs standard buffers of Britton global buffers. Electronic spectra were estimated in Ethanol at 298 K using a Jasco P-530 UV– vis spectrophotometer

3.5 Inspection of magnetic moment measurements

Assessing magnetic susceptibility serves as a sophisticated technique for investigating transition metal coordination compounds, revealing structural characteristics. This approach requires measuring a complex's molar susceptibility while applying diamagnetic corrections to account for non-magnetic components present in the sample. The fundamental objective involves isolating and quantifying the magnetic behavior originating specifically from paramagnetic metal centers within the material. Multiple methodologies exist for calculating these diamagnetic adjustments, among which Pascal's constants provide a frequently utilized theoretical foundation.

$$\mu_{eff} = 2.83\sqrt{X_A.T} \qquad (S1)$$

$$X_A = X_M - (\text{diamagnetic correction}) \qquad (S2)$$

$$X_M = X_g \,.\, M.wt \qquad (S3)$$

The equation being analyzed integrates several parameters: T denotes thermodynamic temperature on the Kelvin scale, μ_{eff} stands for the magnetic moment's effective value measured in Bohr Magnetons (B.M), X_g corresponds to the experimentally determined magnetic susceptibility g-factor, X_M represents the uncorrected molar magnetic permeability, and X_A designates the adjusted molar magnetic permeability following calibration procedures.

3.6. Thermo-gravimetric analysis and kinetic studies

Thermogravimetric analysis (TGA) was employed to evaluate the thermal stability of the complexes and to provide insight into the composition of the final metal oxide residues formed upon decomposition.This technique also quantified the metal content within the compound. Furthermore, the thermally driven decomposition process follows kinetic control, enabling assessment of both kinetic parameters and thermodynamic properties. These analyses were conducted using the Coats-Redfern methodology as detailed below :

$$\ln = \left[\frac{g(\alpha)}{T^2}\right] = \ln\left(\frac{AR}{\beta E}\right) - \frac{E}{RT} \qquad (S4)$$

In which, $g(\alpha) = 1-(1-\alpha)^{1-n}/1-n$ when $n \neq 1$ while, $g(\alpha) = -\ln(1-\alpha)$ at $n = 1$, R is the gas constant. To determine the reaction order (*n*), correlation coefficients (r) were computed via least-squares regression. This involved plotting $\ln[g(\alpha)/T^2]$ against 1/T. The n-value yielding the strongest linear correlation ($r \approx 1$) was designated as the order parameter for each degradation stage. From the resulting linear plot, the pre-exponential factor (A) was derived from the y-intercept. The activation energy (E_a) was calculated using the slope (E_a/R). Subsequently, thermodynamic parameters were evaluated based on (A) and (E_a) using a straightforward computational approach.

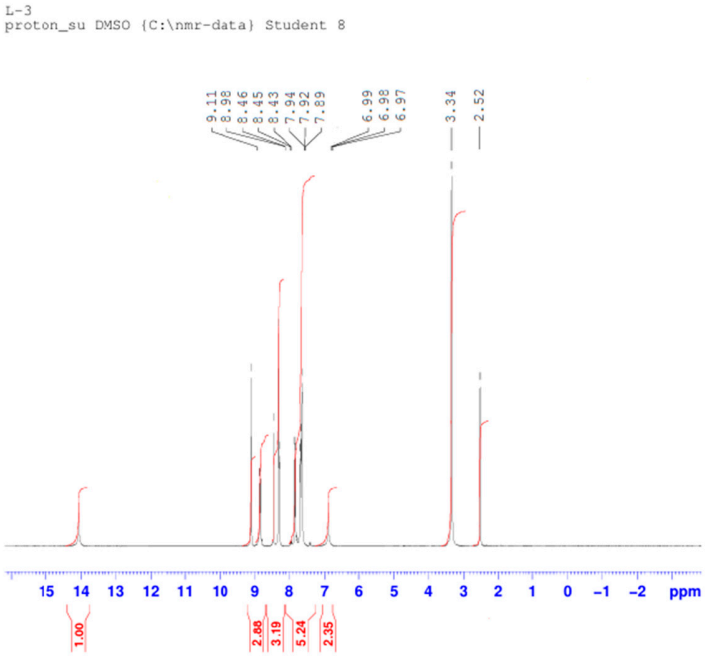
3.8.2. Docking perspective

Molecular docking analyses were performed using the MOE 2019 software suite . Protein crystal structures were retrieved from the Protein Data Bank (PDB) for *Micrococcus luteus* (PDB: 3IF5), *Geotrichum candidum* (PDB: 1THG), and breast cancer cells (PDB: 3HB5). Docking runs were carried out under default parameters, and the optimal conformations were selected based on calculated binding scores,

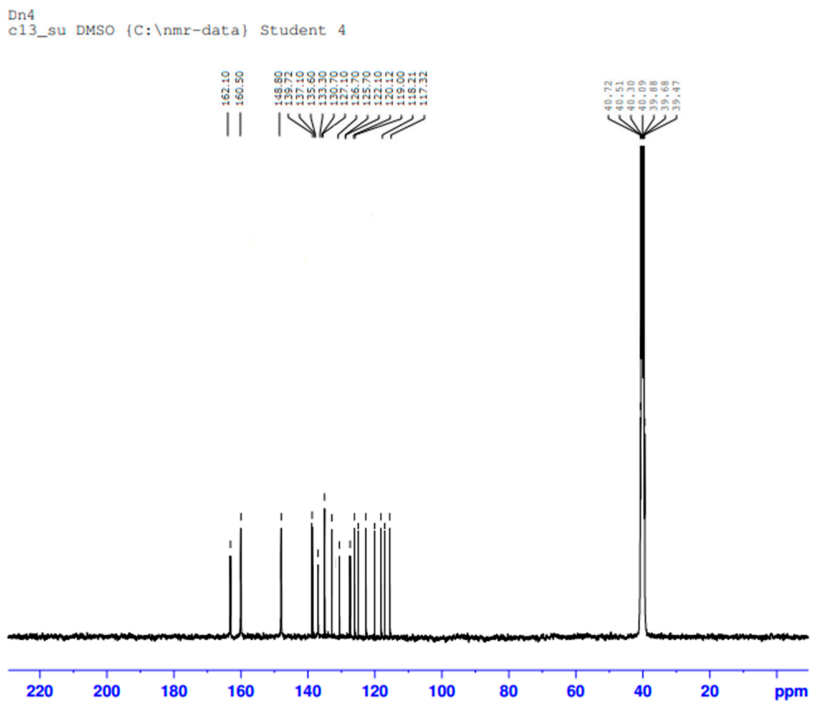
E-values, and favorable interactions between the tested compounds and the key amino acid residues within the target protein receptors.

Agarose gel electrophoresis

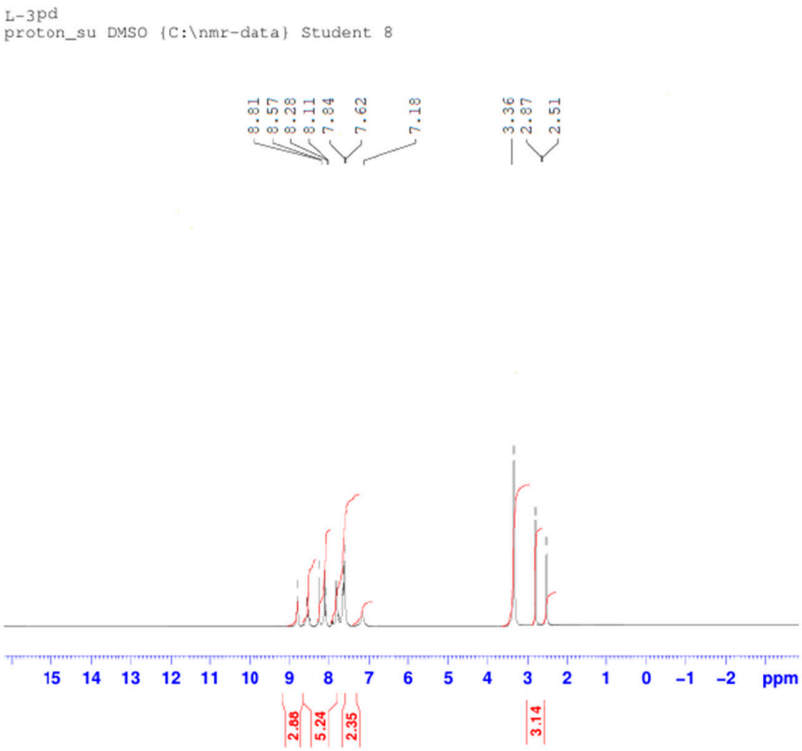
For the majority of compounds analyzed in DMSO solvent, the established procedure involves incubating DNA-containing solutions at 37°C for one hour. A 0.8% agarose gel was cast using 15 mL of freshly prepared Tris-acetate-EDTA (TAE) buffer. Prior to loading the solidified gel, the electrophoresis chamber was filled with TAE buffer. Subsequently, electrophoresis was performed at 100 V for 60 minutes, applying 35 µl of each incubated metal complex-DNA mixture previously combined with bromophenol blue dye in equal proportions. Following termination of the electric current to halt DNA migration, the gel was removed and immersed in a 25 µg/mL ethidium bromide solution for 20–30 minutes for staining. DNA bands were visualized under UV light via a trans-illuminator and documented digitally. DNA degradation levels were quantified by comparison with standard reference markers.



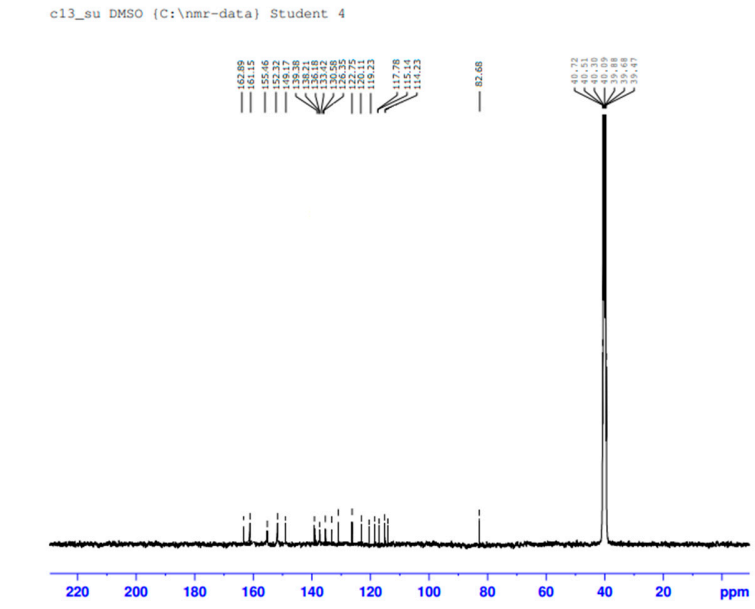
(Fig S1): ^{1}H-NMR of the prepared NQP ligand



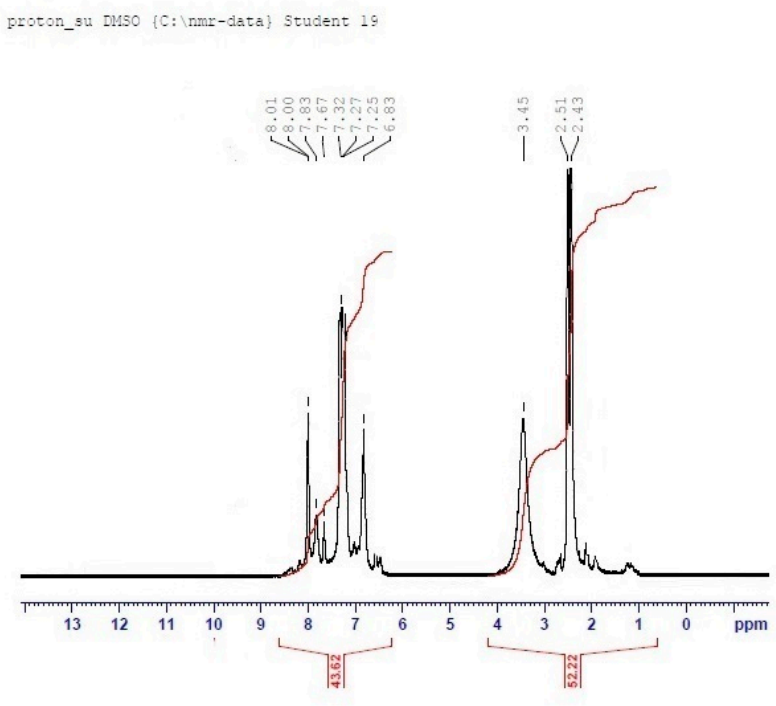
(Fig S2): ^{13}C-NMR of the prepared NQP ligand



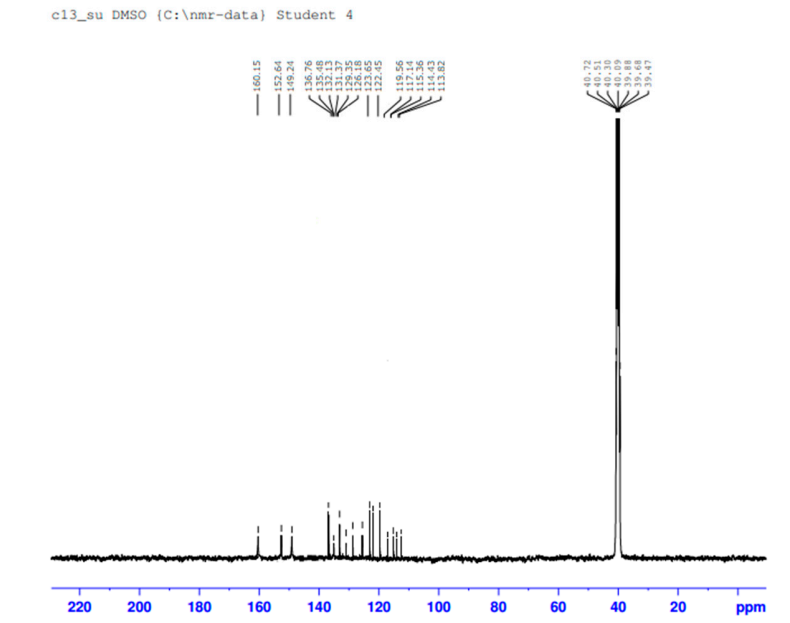
(Fig S3): ^{1}H-NMR of the prepared NQP-Pd complex



(Fig S4): ^{13}C-NMR of the prepared NQP-Pd complex



(Fig S5): ^{1}H-NMR of the prepared NQP-Zn complex



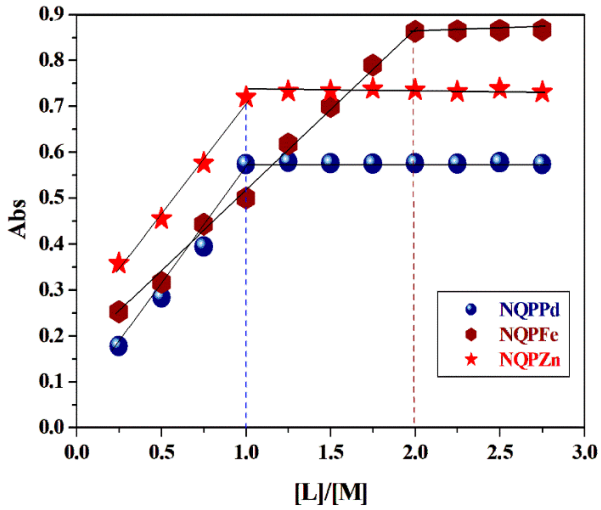
(Fig S6): ^{13}C-NMR of the prepared NQP-Zn complex

Table S1: IR spectra **of the investigated compounds**

IR, Cm^{-1}					
Compound	**υ(OH)/ H_2O**	**υ(C=N)**	**υ(C-O)**	**υ (M-O)**	**υ(M- N)**
NQP	3419	1624	1281	-	-
NQPFe	3449	1611	1255	523	474
NQPZn	3405	1602	1248	566	468
NQPPd	3437	1605	1257	558	497

(Table S2): Molecular electronic spectra, λ_{max} (nm) and ε_{max} (dm^3 $mol^{-1}cm^{-1}$) of the prepared NQP ligand and its complexes in Ethanol at 298 K against Ethanol as a blank

Ligand and its complexes	λ_{max}(nm)	ε_{max} (dm^3 Mol^{-1} cm)	Assignment
NQP	243	1966	$\pi\rightarrow\pi^*$
	293	1851	$n\rightarrow\pi^*$
	304	1760	$n\rightarrow\pi^*$
	395	1861	Intra-ligand
	470	1369	Intra-ligand
NQPFe	277	1424	$\pi\rightarrow\pi^*$
	295	1349	$n\rightarrow\pi^*$
	314	1503	$n\rightarrow\pi^*$
	371	1315	LMCT band
	482	1741	LMCT band
NQPZn	255	1861	$\pi\rightarrow\pi^*$
	329	580	$n\rightarrow\pi^*$
	341	590	LMCT band
	448	203	LMCT band
NQPPd	250	1265	$\pi\rightarrow\pi^*$
	293	948	$n\rightarrow\pi^*$
	307	1342	LMCT band
	399	758	LMCT band
	467	1523	d-d band



(Fig S7): Molar ratio plots for the prepared complexes in Ethanol at[complex]=1×10^{-3}M and 298K

(Table S3): Selected geometric bond lengths, bond angles, and dihedral angles of the optimized ligand NQP and its Pd, Fe, and Zn chelates using B3LYP/6-311G(d,p) and B3LYP/6-311G(d,p)-LANL2DZ level

Compound	Bond lengths (Å)		Bond angles		Dihedral angles	
Ligand (NQP)						
	C3-C4	1.4106	C3-C4-N6	123.900	C3-C4-N6-C5	0.000
	C4-N6	1.3166	C4-N6-C5	119.145	C4-N6-C5-C13	180.000
	N6-C5	1.3593	N6-C5-C13	120.154	N6-C5-C13-N17	0.000
	C5-C13	1.4430	C5-C13-N17	127.356	C5-C13-N17-C18	0.000
	C13-N17	1.4027	C13-N17-C18	126.563	C13-N17-C18-C19	180.000
	N17-C18	1.2940	N17-C18-C19	120.320	N17-C18-C19-C23	0.000
	C18-C19	1.4535	C18-C19-C23	121.821	C18-C19-C23-C24	180.000
	C18-C19	1.4535	C18-C19-C23	121.821	C18-C19-C23-O28	0.000
	O28-C23	1.3282	O28-C23-C19	30.439	O28-C23-C19-C18	180.000
Fe-NQP						
	C3-C4	1.4656	C3-C4-C6	119.517	C3-C4-C6-C5	-10.160
	C3-C4	1.4656	C3-C4-C6	119.517	C3-C4-C6-N13	174.981
	C3-C4	1.4656	C3-C4-N17	128.816	C3-C4-N17-	-172.493

					Fe33	
	C4-C6	1.3328	C4-C6-N13	116.138	C4-C6-N13-C12	170.933
	C4-N17	1.4574	C4-N17-Fe33	125.935	C4-N17-Fe33-O62	-44.694
	C6-N13	1.4066	C6-N13-C12	106.658	C6-N13-C12-C11	-2.328
	C6-N13	1.4066	C6-N13-Fe33	121.874	C6-N13-Fe33-O62	144.439
	N13-Fe33	2.4213	N13-Fe33-O62	63.630	N13-Fe33-O62-C54	108.909
	N13-Fe33	2.4213	N13-Fe33-N50	116.353	N13-Fe33-N50-C51	-22.535
	N13-Fe33	2.4213	N13-Fe33-N36	179.697	N13-Fe33-N36-C37	-170.170
	N13-Fe33	2.4213	N13-Fe33-O32	116.512	N13-Fe33-O32-C21	64.645
	Fe33-N36	2.4230	Fe33-N36-C37	123.546	Fe33-N36-C37-C43	-2.917
	N36-C37	1.4066	N36-C37-C43	117.045	N36-C37-C43-N50	1.981
	C19-C21	1.3813	C19-C21-O32	115.781	C19-C21-O32-Fe33	-28.069
	C21-O32	1.5656	C21-O32-Fe33	23.047	C21-O32-Fe33-N17	-148.350
	O32-Fe33	2.4210	O32-Fe33-N13	116.512	O32-Fe33-N13-C12	160.084
Pd-NQP						
	C3-C4	1.3832	C3-C4-C6	118.308	C3-C4-C6-N13	-179.974
	C4-C6	1.4238	C4-C6-N13	117.937	C4-C6-N13-Pd33	-0.223
	C4-N17	1.4177	C4-N17-Pd33	112.784	C4-N17-Pd33-O32	179.746
	C6-N13	1.36777	C6-N13-Pd33	112.754	C6-N13-Pd33-N17	0.293
	N13-Pd33	2.0468	N13-Pd33-N17	81.519	N13-Pd33-N17-C4	-0.315
	N13-Pd33	2.0468	N13-Pd33-O32	174.269	N13-Pd33-O32-C25	-0.537
	N13-Pd33	2.0468	N13-Pd33-N17	81.519	N13-Pd33-N17-C18	179.772

	N13-Pd33	2.0468	N13-Pd33-O34	85.340	N13-Pd33-O34-C35	-178.968
	C25-O32	1.2826	C25-O32-Pd33	125.648	C25-O32-Pd33-N17	0.064
Zn-NQP						
	C3-C4	1.41255	C3-C4-C6	118.895	C3-C4-C6-N13	179.836
	C3-C4	1.41255	C3-C4-N17	125.488	C3-C4-N17-C18	-9.119
	C4-C6	1.4374	C4-C6-N13	119.700	C4-C6-N13-Zn32	5.181
	C4-N17	1.3795	C4-N17-Zn32	111.326	C4-N17-Zn32-34	-85.859
	C6-N13	1.3725	C6-N13-Zn32	109.101	C6-N13-Zn32-O31	-99.098
	C24-O31	1.3142	C24-O31-Zn33	124.877	C24-O31-Zn33-N13	95.468
	N13-Zn32	2.0427	N13-Zn32-O31	164.860	N13-Zn32-O31-C24	95.468
	Zn32-O31	1.9252	Zn32-O31-C24	124.877	Zn32-O31-C24-C19	-2.353

Table S4. The Natural Bond Orbital charge distribution analysis for the ligand NQP and its metal coordination complexes.

	Ligand (NQP)	Fe-NQP	Pd-NQP	Zn-NQP
N6	-0.487	-0.472	-0.431	-0.686
N17	-0.551	-0.466	-0.473	-0.661
O28	-0.659	-0.771	-0.603	-0.840
Fe	-	1.085	-	-
Pd	-	-	0.694	-
Zn	-	-	-	1.398

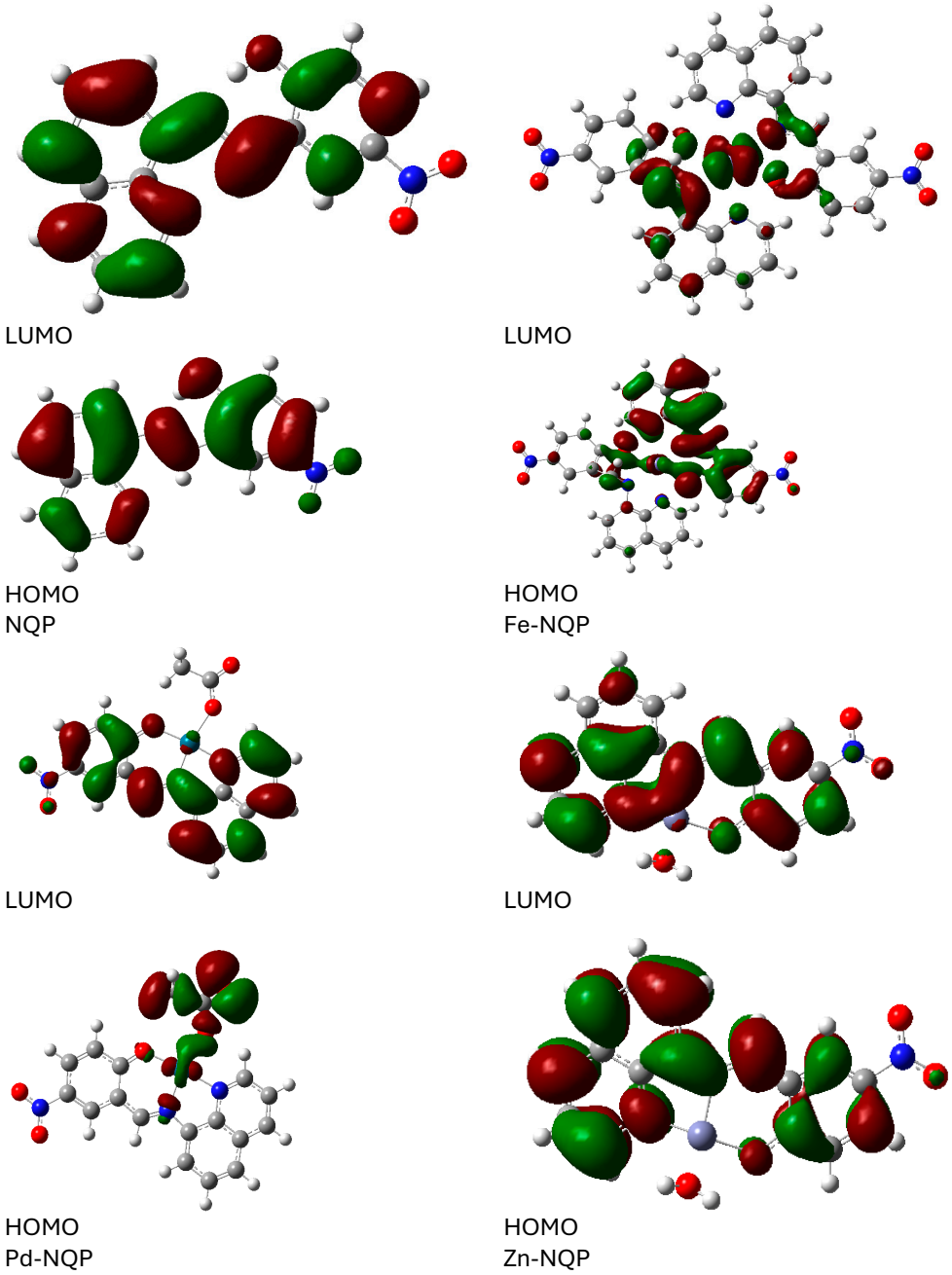
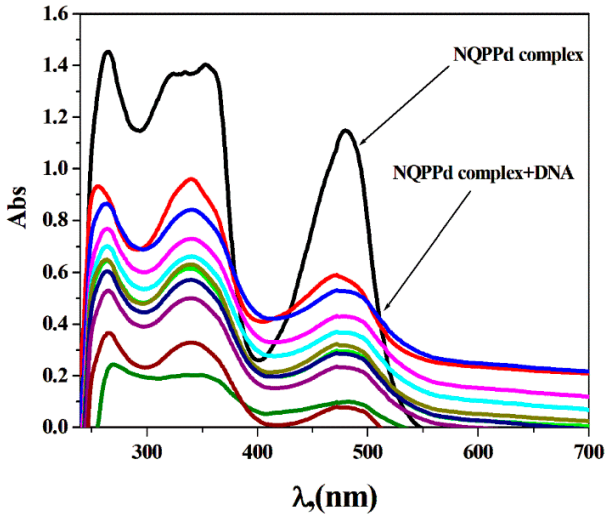


Figure S8: Visualizing Frontier Orbitals: Computational Analysis of NQP Ligand and Its Metal Chelates via DFT Methods.

(Table S5): Calculated natural population, natural charge, and natural electronic configuration of the metal in the studied Pd, Fe, and Zn chelates using B3LYP/6-311G(d,p)-LANL2DZ level

Complex	Natural charge	Core	Natural population			Natural electronic configuration
			Valence	Rydberg	Total	
Fe-NQP	1.0850	17.9964	6.9096	0.0090	24.9150	[core]$4s^{0.21)}3d^{6.44}4p^{0.26}$
Pd-NQP	0.6935	35.9906	9.30662	0.00924	45.3065	[core]$5s^{0.33}4d^{8.75}5p^{0.23}5d^{0.01}$
Zn-NQP	1.3984	18.0000	10.5939	0.0081	28.6016	[core]$4s^{0.33}3d^{9.97}4p^{0.29}$5p0.01



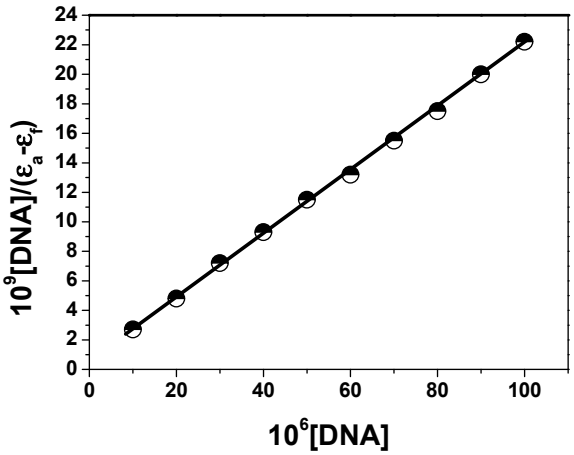
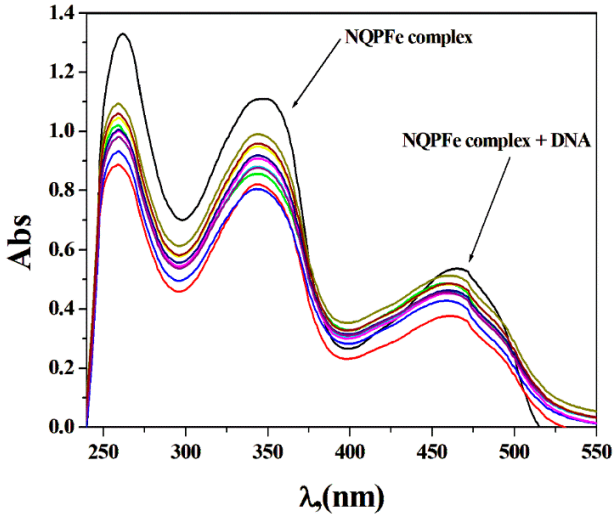


Figure S9: (a) Electronic spectral scans for the binding CT-DNA with NQP-Pd complex (10^{-3} M) in 0.01 M tris buffer (pH = 7.2, 298 K) with CT-DNA (0 –100 μM, from top to bottom). (b): Plot of [DNA] / ($\varepsilon_a - \varepsilon_f$) versus [DNA] for the interaction CT-DNA with NQP-Pd complex



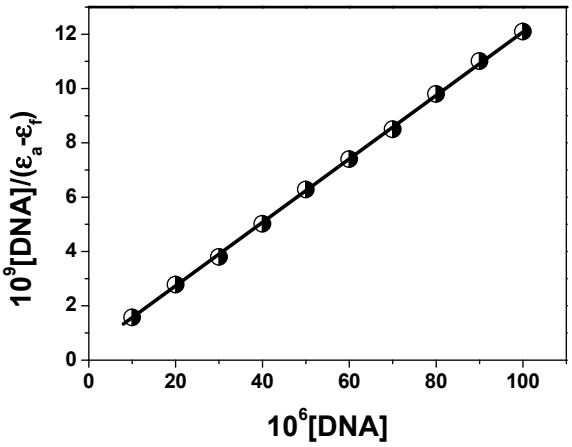


Figure S10: (a) Electronic spectral scans for the binding CT-DNA with NQPFe complex (10^{-3} M) in 0.01 M tris buffer (pH = 7.2, 298 K) with CT-DNA (0 –100 μM, from top to bottom). (b) Plot of [DNA] / ($\varepsilon_a - \varepsilon_f$) versus [DNA] for the interaction CT-DNA with NQP-Fe complex

Table S6: Results of antimicrobial bioassay of the titled compounds against different strains of bacteria and Fungi

Compounds	Inhibition zone (mm) ± SD											
	Serratia Marcescence (-ve)		*Escherichia Coli (-ve)*		*Micrococcus Luteus (+ve)*		*Aspergillus Flavus*		*Getrichm Candidum*		*Fusarium Oxysporum*	
Conc. (µg/ml)	**10**	**15**	**10**	**15**	**10**	**15**	**10**	**15**	**10**	**15**	**10**	**15**
NQP	6.50±0.12	9.75±0.14	±0.07 4.30	7.50±0.08	9.4±0.10	13.5±0.09	4.75±0.06	7.0±0.09	7.4±0.03	12.5±0.16	6.3±0.07	10.2±0.12
NQPPd	17.5±0.13	26.5±0.10	12.4±0.11	22.7±0.12	20.4±0.15	37.60±0.16	10.60±0.12	17.8±0.06	16±0.17.4	33.4±0.13	11.2±0.05	20.9±0.14
NQPFe	14.2±0.13	22.9±0.14	9.75±0.10	18.4±0.13	17.1±0.07	34.4±0.10	8.75.0±0.03	14.1±0.13	13.8.0±0.10	29.5±0.17	9.7±0.03	17.5±0.11
NQPZn	16.20±0.17	24.80±0.13	10.0±0.07	20.6±0.15	18.5±0.13	35.8±0.20	9.5±0.08	15.9±0.10	15.5±0.14	31.2±0.17	10.5±0.16	19.3±0.10
Ofloxacin	18.5±0.11	28.7±0.12	14.3±0.02	24.7±0.15	24.5±0.13	40.5±0.09						
Fluconazol							12.4±0.09	19.5±0.14	20.4±0.15	35.5±0.17	12.75±0.13	22.6±0.15

Table S7. Percentage activity index results for antimicrobial assessment of the NQP azomethine ligand and its corresponding complexes

Compound	**Activity index (%)**					
	Bacteria				**Fungi**	
	S. marcescence	***E. coli***	***M. luteus***	***A. flavus***	***G. candidum***	***F. oxysporum***
NQP	33.97	30.36	33.33	35.90	35.21	45.13
NQPPd	92.33	91.90	92.83	91.28	94.08	92.48
NQPFe	79.79	74.49	84.94	72.31	83.10	77.43
NQPZn	86.41	83.40	88.40	81.54	87.89	85.40

(Table S8): Cytotoxic activity (IC_{50}) of the prepared imine ligands and their complexes against colon carcinoma cells, (HCT-116 cell line), hepatic cellular carcinoma cells, (HepG-2) and breast

Compounds	IC_{50}(µg/µl)		
	MCF-7	HCT-116	HepG-2
NQP	75.06±0.15	90.45±0.13	82.65±0.14
NQPPd	6.35±0.04	12.95±0.14	7.45±0.13
NQPFe	10.11±0.05	17.50±0.07	12.56±0.09
NQPZn	8.25±0.15	14.70±0.19	9.25±0.13
cisplatin	8.28±0.14	10.65±0.12	6.45±0.08

(Table S9): Anti-oxidant activity of the prepared compounds

Complex	IC50
NQP	61.20±0.08
NQPPd	18.70±0.12
NQPFe	26.40±0.10
NQPZn	22.35±0.12
Ascorbic acid	50.70±0.14

(Table S10): The Docking interaction data calculations of the NQP ligand and its complexes with the active site of the receptor of *Micrococcus luteus* (BDB ID: 3IF5), *Geotrichum candidum* (PDB ID: 1THG, and *Breast cancer* (BDP ID: 3HB5)

System	Binding score (kcal/mol)	Receptor	Interaction	Distance(Å)	E (kcal/mol)
***Getrichum candidum* (PDB ID: 1THG)**					
NQP-1THG					
O 29	-9.67	OG1 THR 166	H-donor	2.99	-1.9
O 32		N SER 137	H-acceptor	3.08	-1.3
O 33		OH TYR 141	H-acceptor	3.26	-1.1
Fe-NQP-1THG					
O 65	-7.53	OG SER 137	H-acceptor	2.87	-1.0
Pd-NQP-1THG					
O 41	-8.42	N GLY 131	H-acceptor	3.30	-1.0
O 41		OH TYR 141	H-acceptor	2.99	-2.2
O 42		N SER 137	H-acceptor	2.88	-1.0

Zn-NQP-1THG **N 30** **O 36** **O 36** **O 37**	-8.08	O ALA 132 N GLY 131 OH TYR 141 N SER 137	H-donor H-acceptor H-acceptor H-acceptor	3.32 3.24 3.26 2.91	-2.6 -0.8 -1.1 -2.0
***Micrococcus luteus* (PDB ID: 3IF5)**					
NQP-3IF5 **O 29** **O 32** **6-ring**	-6.68	OD1 ASN 152 N VAL 188 CG1 VAL 225	H-donor H-acceptor pi-H	2.79 3.20 3.94	-0.9 -2.0 -0.9
Fe-NQP-3IF5 **O 65**	-4.63	OG SER 235	H-acceptor	3.06	-1.7
Pd-NQP-3IF5					
-	-5.49	-	-	-	-
Zn-NQP-3IF5					
N 10 **O 33**	-4.70	OG SER 227 OD2 ASP 419	H-donor H-donor	3.23 2.93	-1.6 -4.2
***Breast cancer* (BDP ID: 3HB5)**					
NQP-3HB5 **O 29** **O 32** **6-ring**	-6.68	OD1 ASN 152 N VAL 188 CG1 VAL 225	H-donor H-acceptor pi-H	2.79 3.20 3.94	-0.9 -2.1 -0.9
Fe-NQP-3HB5					
-	0.25	-	-	-	-
Pd-NQP-3HB5 -	-6.75	-	-	-	-
Zn-NQP-3HB5					
O 33	-6.43	O ASN 90	H-donor	3.53	-0.8
6-ring		6-ring PHE 192	pi-pi	3.99	-0.0

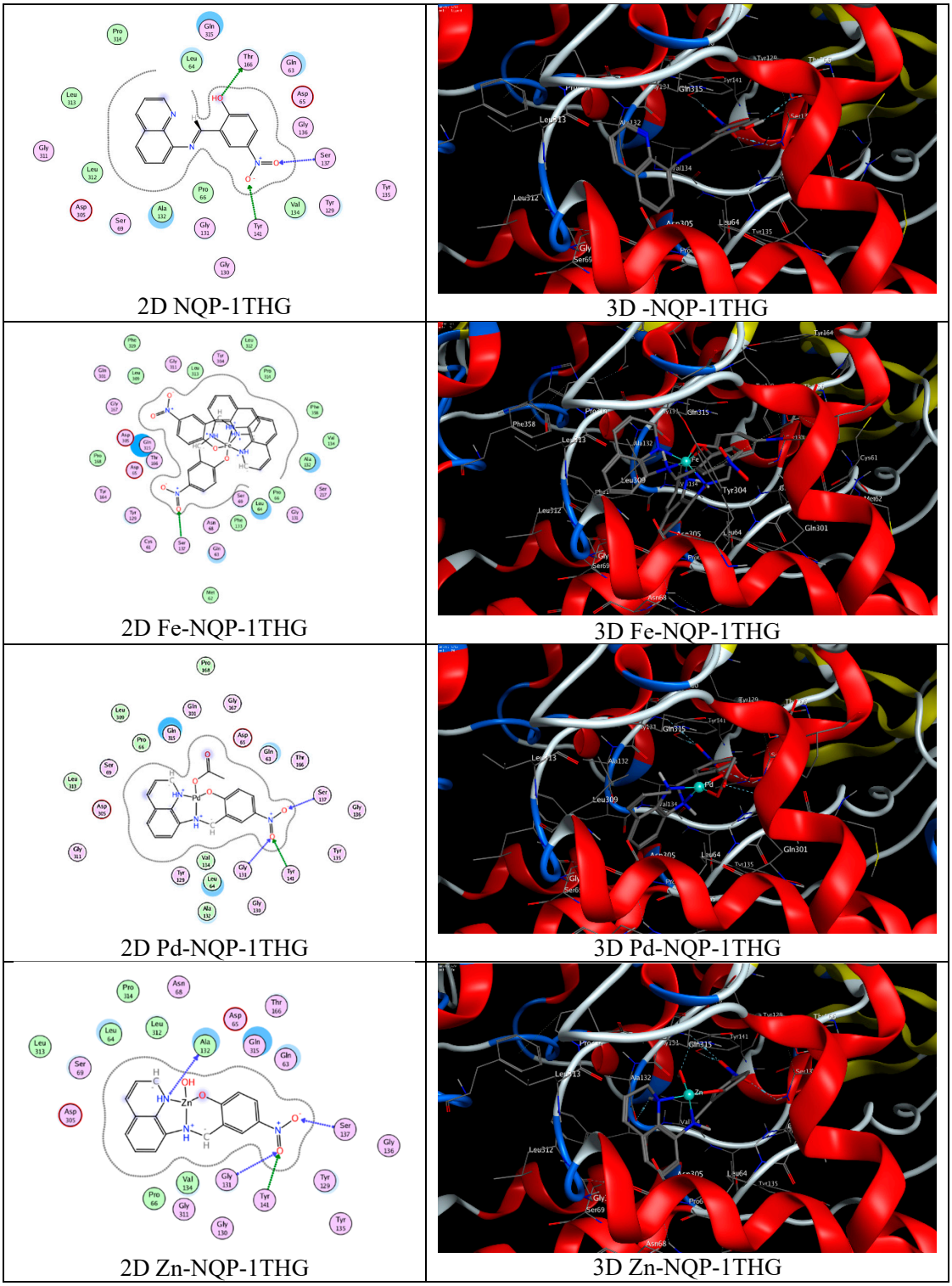


Figure S11: Molecular docking simulation studies of the interaction between the investigated NQP ligand and its chelates with the active site of the receptor of *Geotrichum candidum* (PDB ID: 1THG)